Construction of functional neural network tissue combining CBD-NT3-modified linear-ordered collagen scaffold and TrkC-modified iPSC-derived neural stem cells for spinal cord injury repair

Zhaoping Wu [a,b,1], Yi Zhou [a,b,1], Xianglin Hou [c], Weidong Liu [a,d,e], Wen Yin [a,b], Lei Wang [a,d,e], Yudong Cao [a,b], Zhipeng Jiang [a,b], Youwei Guo [a,b], Quan Chen [a,b], Wen Xie [d,e], Ziqiang Wang [f], Ning Shi [d,e,g], Yujun Liu [g], Xiang Gao [g,*****], Longlong Luo [g,****], Jianwu Dai [c,***], Caiping Ren [a,b,d,e,**], Xingjun Jiang [a,b,*]

[a] Department of Neurosurgery, Xiangya Hospital, Central South University, Changsha, Hunan Province, 410008, China
[b] National Clinical Research Center for Geriatric Disorders, Xiangya Hospital, Central South University, Changsha, Hunan Province, 410008, China
[c] State Key Laboratory of Molecular Developmental Biology Institute of Genetics and Developmental Biology, Chinese Academy of Sciences, Beijing, 100080, China
[d] School of Basic Medical Science, Central South University, Changsha, Hunan Province, 410078, China
[e] The NHC Key Laboratory of Carcinogenesis and the Key Laboratory of Carcinogenesis and Cancer Invasion of the Chinese Ministry of Education, Central South University, Changsha, Hunan Province, 410078, China
[f] College of Biology, Hunan University, Changsha, 410000, China
[g] State Key Laboratory of Toxicology and Medical Countermeasures, Beijing Institute of Pharmacology and Toxicology, Beijing, 100080, China

ARTICLE INFO

ABSTRACT

Induced pluripotent stem cells (iPSCs) can be personalized and differentiated into neural stem cells (NSCs), thereby effectively providing a source of transplanted cells for spinal cord injury (SCI). To further improve the repair efficiency of SCI, we designed a functional neural network tissue based on TrkC-modified iPSC-derived NSCs and a CBD-NT3-modified linear-ordered collagen scaffold (LOCS). We confirmed that transplantation of this tissue regenerated neurons and synapses, improved the microenvironment of the injured area, enhanced remodeling of the extracellular matrix, and promoted functional recovery of the hind limbs in a rat SCI model with complete transection. RNA sequencing and metabolomic analyses also confirmed the repair effect of this tissue from multiple perspectives and revealed its potential mechanism for treating SCI. Together, we constructed a functional neural network tissue using human iPSCs-derived NSCs as seed cells based on the interaction of receptors and ligands for the first time. This tissue can effectively improve the therapeutic effect of SCI, thus confirming the feasibility of human iPSCs-derived NSCs and LOCS for SCI repair and providing a valuable direction for SCI research.

1. Introduction

Spinal cord injury (SCI) is a common and severe injury of the central nervous system (CNS) that leads to neurological dysfunction below the plane of injury [1,2]. Lacking of effective treatment, SCI is a devastating disease with high morbidity and even may be fatal [3,4]. Primary trauma, scar formation, and deterioration of the microenvironment caused by inflammation, ischemia, and other factors lead to poor

prognosis of SCI [5]. The regeneration of additional neurons in the injured area and formation of an increasingly complete neural circuit are keys to SCI treatment [2].

Conductive biomaterials may be a linchpin that empowers the synergy between regenerative medicine and rehabilitation approaches for SCI [6]. Collagen material was applied in SCI repair because of its abundance, good plasticity and great biocompatibility. In this study, we used a collagen scaffold named linear-ordered collagen scaffold (LOCS) [7] which was made from bovine aponeurosis and the manufacturing process was described in previous study [8]. The implantation of LOCS in SCI models can promote the accumulation of stem cells in the SCI area, inhibit the formation of glial scars [9], provide support for neuronal growth and axon extension in a directed manner [10,11]. In addition, by modifying factors such as neurotrophin-3 (NT3), BDNF, and VEGF to add collagen-binding domain (CBD), these factors can bind to the LOCS more effectively and continue to function in the spinal cord areas [12,13]. LOCS are also useful carriers for drugs or exogenously transplanted cells [14–16].

Neural stem cells (NSCs) are cells that can self-renew and differentiate into neurons and glial cells through asymmetric division [17]. NSCs are considered to play an important role in the treatment of SCI, but the number of endogenous NSCs accumulated in the SCI area is limited [18]. Exogenous NSCs for transplantation are difficult to be obtained and may be ethically problematic. Therefore, we considered the use of pluripotent stem cell-derived NSCs for SCI treatment [19]. Induced pluripotent stem cells (iPSCs) are pluripotent, self-renewing cells that are reprogrammed from terminally differentiated somatic cells. iPSCs have strong proliferation and differentiation abilities, can be derived from patients individually [20,21], and can be used for cell transplantation therapy in SCI [22].

Being affected by the spinal cord environment, such as cerebrospinal fluid circulation, transplanted cells have difficulty surviving and growing in the SCI areas. Therefore, we aimed to construct a functional neural network tissue based on iPSC-derived NSCs and LOCS. Since NT3 specifically binds to tyrosine receptor kinase C (TrkC) to promote axon generation, neuronal differentiation and survival [23,24], we overexpressed TrkC in iPSCs. After inducing iPSCs-TrkC differentiation into NSCs, they were combined with LOCS loaded with CBD-NT3. We assume that this functional neural network tissue based on iPSC-derived cells, LOCS, and factors may provide a solution for individualized acquisition of NSCs and allow additional NSCs to plant, directionally expand, and differentiate in the SCI area. We thus investigated the effects of this functional neural network tissue on SCI regeneration in a rat SCI model with complete transection. The experimental procedure used in this study is shown in Fig. 1.

2. Materials and methods

2.1. Ethics

In this study, we used Sprague-Dawley (SD) rats to construct a complete transection SCI model. All animal experiments were conducted in compliance with the Chinese Ministry of Public Health Guide for Animal Ethics and Welfare. This study was approved by the Ethics Committee of the Xiangya Hospital of Central South University and the Department of Laboratory Animals of Central South University. Ethics No. CSU-2022-01-0099.

2.2. Human iPSC culture

The iPSCs (Nuwacell, China) used in this study were derived from the human umbilical cord. iPSCs culture was performed using the npEpic system (Nuwacell, China) on plates coated with Matrigel (Corning, USA). Matrigel was diluted using DMEM/F12 (BI, Israel), incubated cell culture plates in 37 °C for 2 h before passaging. iPSCs were passaged every 4–5 days using EDTA dissociation buffer (Gibco, USA). The

dispersed cells were collected, aspirated in npEpic medium, and replated at a 1:4–1:6 ratio [25].

2.3. Construction of iPSC-TrkC cell line

To overexpress TrkC, iPSCs were infected with lentiviruses expressing TrkC and puromycin resistance (WZ Biosciences Inc., Shandong, China) at a multiplicity of infection (MOI) of 50. After 72 h, culture medium containing puromycin was added, and the puromycin culture medium was replaced daily. Finally, three iPSC-TrkC cell lines were established. We used RT-qPCR and Western Blot to detect TrkC expression in all the three cell lines. The iPSC-TrkC cell line with the highest TrkC expression was used in subsequent experiments.

2.4. Differentiation of iPSC-TrkC into iPS-NSCs-TrkC

We induced iPSC-TrkCs to differentiate into NSCs using a neural induction medium (Gibco, USA). At approximately 24 h before induction, iPSC-TrkC were passaged and were in an ideal cellular state, with a cell growth confluence of 15–20 %. Neural induction medium was added and replaced daily. After seven days, the cells possessed the basic characteristics of NSCs, and we passaged the cells into new plates and changed the induction medium to NSCs culture medium. The NSC culture medium consisted of Knockout DMEM/F12, basic fibroblast growth factor (bFGF, Peprotech, USA), epidermal growth factor (EGF, Peprotech, USA), StemPro neural supplement (Gibco, USA), and GlutaMax (Gibco, USA). iPS-NSCs-TrkC were passaged every 4–5 days using Accutase (Invitrogen, USA).

We also used a neural induction medium to differentiate iPSCs into iPS-NSCs for subsequent control group experiments. The methods for differentiation and cell culture were as same as described above.

2.5. RT-qPCR

TRIzol (Invitrogen, USA) was used to extract RNA from the cells. The RevertAid RT Reverse Transcription Kit (Thermo Scientific, Waltham, MA, USA) was used to convert the RNA to cDNA. The RT-qPCR data were analyzed using the $2^{-\Delta\Delta Ct}$ strategy, and values were relative to the housekeeping gene Glyceraldehyde-3-Phosphate Dehydrogenase (GAPDH). A complete list of primers used is provided in Table S1.

2.6. Pretreatment of LOCS, seeding of iPS-NSCs and iPS-NSCs-TrkC

LOCS (NeuroRegen®, DB WUDEREGEN BIOMEDICAL TECHNOLO-GIES (JIANG SU) Co., Ltd, China) were produced from bovine aponeurosis using the method described in our previous report [26]. The standards for the LOCS were established and tested by the National Institute of Food and Drug Control according to the Chinese Criteria for Medical Devices. In this study, the utilized LOCS were 3 mm long and 2 mm in diameter for each bundle. CBD-NT3 is a recombinant fusion protein consisting of NT3 and CBD, designed to strengthen the binding ability to collagen materials. The preparation methods were described in our previous article [12]. In simple terms, CBD is a peptide with the sequence TKKTLRT, which exhibits strong binding affinity to type I collagen. The coding sequence of TKKTLRT is fused with the NT3 coding sequence to obtain the CBD-NT3 coding sequence, which is then expressed in cells and purified to obtain the CBD-NT3 protein (17.69 kD). LOCS is a type I collagen material, and CBD-NT3 can bind to LOCS through its CBD domain, thus stabilizing on LOCS.To further explore the advantages and effects of nerve regeneration of the spinal cord-like tissue based on iPS-NSCs-TrkC, LOCS, and CBD-NT3, we designed five experimental groups: blank (blank), LOCS combined with CBD-NT3 (LOCS+NT3), LOCS with iPS-NSCs-TrkC (LOCS+NSC-TrkC), LOCS+NT3 with iPS-NSCs (LOCS+NT3+NSC), and LOCS+NT3 with iPS-NSCs-TrkC (LOCS+NT3+NSC-TrkC). To combine LOCS and CBD-NT3, we added 50 μl protein solution containing 5 μg CBD-NT3 in
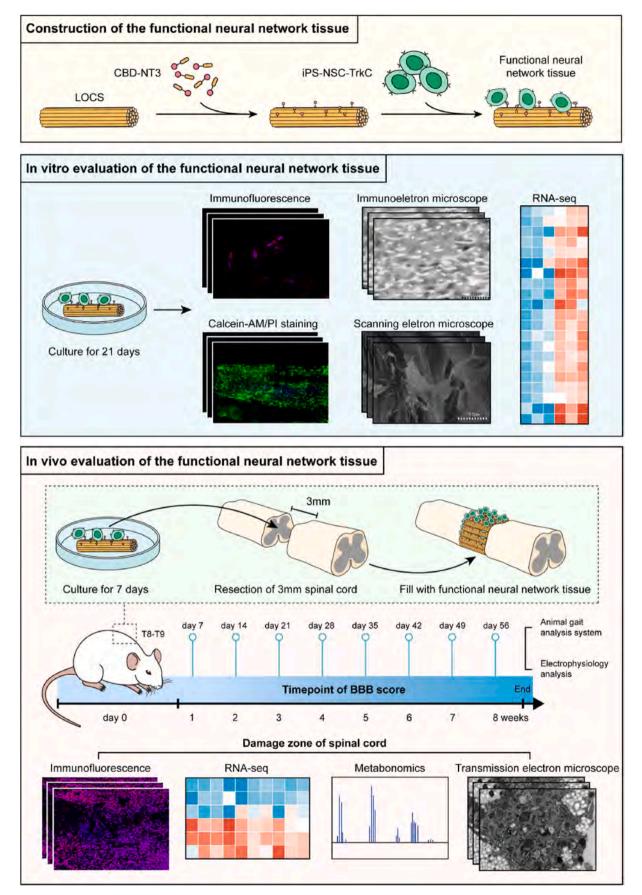
Fig. 1. Flowchart of this experiment.

each bundle of LOCS and incubated the materials in 37 °C for 2 h.

Before seeding the cells, the LOCS and LOCS+NT3 were infiltrated with the NSCs culture medium for 2 h. Each bundle of collagen scaffolds was then seeded with 5×10^5 iPS-NSCs or iPS-NSCs-TrkC according to the different groups. After dropping the cell suspension, the collagen scaffolds were incubated on low-adhesion cell culture plates in a cell incubator for 6 h. A sufficient amount of NSC culture medium was added for subsequent long-term culturing.

2.7. Live/dead cell assay

Calcium-AM (Beyotime, C2015, 1:1000) and propidium iodide (PI, Beyotime, C2015, 1:1000) were added to the cell culture medium to prepare the Live/Dead assay working solution. After adding the working solution, the materials were incubated at 37 °C for 30 min. Following nuclear staining with Hoechst 33342 (Beyotime, C1027, 1:1000), the materials were observed using fluorescence microscopy.

2.8. Western Blot analysis

Equal amounts of protein were separated by 7.5 % sodium dodecyl sulfate-polyacrylamide gel electrophoresis (SDS-PAGE), and the proteins were transferred to a polyvinylidene fluoride (PVDF) membrane at a constant voltage of 100V. After blocking, the membrane was sequentially incubated with primary and secondary antibodies. The following antibodies were used: GAPDH (Proteintech, 60004-1-Ig, 1:5000), TrkC (Proteintech, 66380-1-Ig, 1:2000), pTrkC (Abcam, ab197071, 1:2000). The Bio-Rad Image Lab software was used for Western Blot imaging analysis.

2.9. Animals and surgical procedures

In this study, we used 50 six-week-old female SD rats to construct T8-T9 complete transection SCI models with microsurgery. The rats were fed for 8 weeks after surgery. All surgical procedures were performed under intraperitoneal anesthesia with Zoletil (75 mg/kg) and xylazine (10 mg/kg), and isoflurane inhalation was used to assist with anesthesia, if necessary. After anesthesia, a 1.5 cm long skin midline incision was made, and the subcutaneous and muscular tissues were separated laterally. Laminectomy was performed at the T8-T9 vertebral level. A 3 mm long transection was performed using a 15° stab knife (SharPoint, USA) at T8-T9 spinal cord. The bleeding at the SCI area was controlled with gelatin sponge. LOCS treated using different methods were transplanted into the SCI area to ensure that the direction of the scaffold was parallel to that of the spinal cord. The blank group was not subjected to any material transplantation. The dissected spinal meninges, muscle and skin layers were sutured carefully and the rats were closely observed until they recovered from anesthesia. All rats received postoperative care, including an intramuscular penicillin injection of 40,000 units per rat per day for 5 d and assisted urination until they were able to urinate autonomously.

2.10. Behavior analysis

The hind limb movements of the rats were observed immediately and weekly after surgery. The Basso, Beattie, and Bresnahan locomotor rating scale (BBB scale) was used by two experimenters who were blinded to the rat groups to evaluate hind limb function. We conducted the inclined grid climbing test to assess the recovery of hind limb motor function and coordination, which could differentiate local reflex activity from voluntary movement. We further used an animal gait analysis system to measure the step order and load-bearing state of the rats' hind limb movements during walking. The system recording method required the rats to successfully land on the palm side of their hind limbs and walk a distance, and only the recovery of the rats in the LOCS+NT3+NSC-TrkC group met this requirement. Therefore, in this analysis, we used

normal rats as a reference. The system analyzed the weight-bearing status of each rat claw, the step sequence, and the corresponding dwell intensity curve.

2.11. Electrophysiology analysis

The evoked potential apparatus used was the M − 800 NeuroExam (MEDCOM Technology, China). Isoflurane inhalation was used to maintain anesthesia in the rats. Stimulating electrodes were placed in the extracranial projection area of the motor cortex and oral cavity. The receiving and grounding electrodes were placed in the gastrocnemius and subcutaneous tissues near the L1 spinal segment, respectively. We used a constant current of 10 mA for single-pulse stimulation at least five times for each rat to obtain a morphologically stable waveform.

2.12. Ultrastructural pathology analysis

All electron microscopy specimens were fixed with 2.5 % glutaraldehyde. An NT3 antibody (Proteintech 18084-1-AP, 1:100) was used for immunoelectron microscopy (IEM) analysis. The sampling location of transmission electron microscope (TEM) was the central region of the SCI area. The images of scanning electron microscope (SEM) and IEM were performed using a Hitachi S-3400 N microscope (Tokyo, Japan). The TEM images were acquired using a Hitachi HT7700 instrument (Tokyo, Japan).

2.13. Immunofluorescence

LOCS seeded with in vitro cultured cells were fixed with 4 % paraformaldehyde (PFA) and sectioned after paraffin embedding. Spinal cord samples from the rats were removed immediately after infusion with 4 % PFA and sectioned after paraffin embedding. The following antibodies were used for immunofluorescence: Nestin (Proteintech, 29285-1-AP, 1:200), Sox2 (Proteintech, 11064-1-AP, 1:200), TrkC (Proteintech, 66380-1-Ig, 1:100), HNA (Abcam, ab191181, 1:100), GFAP (Proteintech, 16825-1-AP, 1:200), Tuj-1 (Abcam, ab18207, 1:100), Map-2 (Proteintech, 17490-1-AP, 1:100), NeuN (Abcam, ab177487, 1:100), MBP (Proteintech, 10458-1-AP, 1:100), Syn (Proteintech, 17785-1-AP, 1:100), PSD95 (Proteintech, 20665-1-AP, 1:100), 5-HT (Sigma-Aldrich, S5545, 1:1000), ChAT (Proteintech, 20747-1-AP, 1:200), VGLUT1 (Proteintech, 55491-1-AP, 1:200), CD68 (Abcam, ab283654, 1:100), NG2 (Abcam, ab275024, 1:100), Laminin (Proteintech, 23498-1-AP, 1:200), Integrin beta 1 (Abcam, ab179471, 1:100). Alexa Fluor™ 488 Goat anti-Rabbit IgG (H+L) Cross-Adsorbed Secondary Antibody (Invitrogen, A-11008, 1:500); Alexa Fluor™ 594 Goat anti-Mouse IgG (H+L) Cross-Adsorbed Secondary Antibody (Invitrogen, A-11005, 1:500). DAPI (Beyotime, C1002, 1:500) was used for nuclear staining.

2.14. RNA sequencing and metabolomics analysis

Total RNA was extracted from cells and spinal cord tissues by using TRIzol. Then RNA quality was determined by 5300 Bioanalyser (Agilent) and quantified using the ND-2000 (NanoDrop Technologies). RNA purification, reverse transcription, library construction and sequencing were performed at Shanghai Majorbio Bio-pharm Biotechnology (Shanghai, China). The RNA-seq transcriptome library was prepared following Illumina® Stranded mRNA Prep, Ligation from Illumina (San Diego, USA) using 1 μg of total RNA. After quantified by Qubit 4.0, paired-end RNA-seq sequencing library was sequenced with the NovaSeq 6000 sequencer (2 × 150bp read length). The raw paired-end reads were trimmed and quality controlled by fastp [27] with default parameters. Then clean reads were separately aligned to reference genome with orientation mode using HISAT2 [28] software. The mapped reads of each sample were assembled by StringTie [29] in a reference-based approach.

For metabolomics analysis, we cut off 50 mg spinal cord tissue from SCI area of each rat. 400 µL of extraction solution (methanol: water = 4:1 (v:v)) containing 0.02 mg/mL of internal standard (L-2-chlorophenylalanine) was used for metabolite extraction. As a part of the system conditioning and quality control process, a pooled quality control (QC) sample was prepared by mixing equal volumes of all samples. The QC samples were disposed and tested in the same manner as the analytic samples. It helped to represent the whole sample set, which would be injected at regular intervals (every 5–15 samples) in order to monitor the stability of the analysis. The LC-MS/MS analysis of sample was conducted on a Thermo UHPLC-Q Exactive HF-X system equipped with an ACQUITY HSS T3 column (Waters, USA) at Majorbio Bio-Pharm Technology (Shanghai, China). The pretreatment of LC/MS raw data was performed by Progenesis QI (Waters, USA) software, and a three-dimensional data matrix in CSV format was exported. The information in this three-dimensional matrix included: sample information, metabolite name and mass spectral response intensity. Internal standard peaks, as well as any known false positive peaks (including noise, column bleed, and derivatized reagent peaks), were removed from the data matrix, de-redundant and peak pooled. At the same time, the metabolites were identified by searching database, and the main databases were the HMDB (http://www.hmdb.ca/), Metlin (https://metlin.scripps.edu/) and Majorbio Database.

2.15. Statistical analysis

We used the Student's t-test, Kruskal–Wallis test, ANOVA, gene set variation analysis (GSVA), and principal components analysis (PCA) in this study. Transcripts Per Million (TPM) method were used to standardize the RNA sequencing data. All statistical analyses were performed using R software (version 4.1.0).

3. Results

3.1. Construction of functional neural network tissue based on LOCS and iPSCs

A diagram of the functional neural network tissue construction is shown in Fig. 2A. To further explore the effect of CBD-NT3 and TrkC on the construction of functional neural network tissues in vitro, we designed LOCS without CBD-NT3 modification and iPSC-NSCs without TrkC overexpression as two control groups. iPSCs overexpressing TrkC by lentiviral transfection were induced to differentiate into NSCs using a neural induction medium (Figs. S1A–D). Immunofluorescence was used to detect Nestin and Sox2 markers, which confirmed that iPSCs differentiated into NSCs. The positive staining of TrkC confirmed that NSCs differentiated from iPSCs maintained TrkC overexpression (Fig. 2B–C).

LOCS were produced as described in our previous report [26], which were 4 cm long and 4 mm in diameter sterilized bundles of collagenous tissue (Fig. 2D). LOCS can be divided into appropriate specifications for SCI transplantation. The morphology of LOCS observed by SEM is shown in Fig. 2E. After incubating CBD-NT3 with LOCS, we used IEM to detect the combination between CBD-NT3 and the LOCS. The nanogold secondary antibody bound to the NT3 antibody, demonstrating the attachment position of CBD-NT3 on the LOCS using electron microscopy (Fig. 2G). To ascertain whether CBD-NT3 can bind to TrkC on the cell membrane, CBD-NT3 was added into the cultured cells at a final concentration of 20 nM. After a 30-min incubation, cells were fixed using 4 % PFA, and the expression of NT3 and TrkC was examined through immunofluorescence. Subsequently, we observed co-localization of NT3 and TrkC in some of the cells (Figs. S1E–F). To further substantiate the evidence showing CBD-NT3's binding with cells, Western Blot experiment was conducted by extracting cellular proteins 6 h after the addition of CBD-NT3. In comparison to iPS-NSCs-TrkC cells without CDB-NT3 treatment, the phosphorylation level of TrkC in CDB-NT3-treated iPS-NSCs-TrkC cells significantly increased. This confirms that CBD-NT3 can bind to TrkC expressed on the cell surface and activate the NT3/TrkC pathway (Fig. 2F).

These results confirmed that NSCs overexpressing TrkC were obtained from iPSCs, and that CBD-NT3 was bound to the LOCS uniformly. We constructed a functional neural network tissue by seeding iPS-NSCs-TrkC on a CBD-NT3-modified LOCS for subsequent experiments.

3.2. CBD-NT3-modified LOCS promotes the survival and proliferation of iPS-NSCs-TrkC

After seeding cells on LOCS and three-dimensional (3D) culturing in vitro, we used Calcein-AM/PI staining to determine the survival status of the cells on the LOCS of each group at day 1, day 7 and day 21. Calcein-AM can be hydrolyzed in cells to produce calcein with a strong green fluorescence, which can be used to trace living cells. And PI, with its red fluorescence, can indicate dead cells. Based on the fluorescence of calcein and PI, we found that TrkC-modified iPSC-derived NSCs adhered to CBD-NT3-modified LOCS and survived. At day 1 (Figs. S1H–J) and day 7 (Fig. S1K-M) in vitro cultivation, the cell density and morphology were better than those of the control groups, in which the LOCS was not modified with CBD-NT3 (LOCS+NSC-TrkC group), or iPSC-NSCs did not overexpress TrkC (LOCS+NT3+NSC group). In addition, the cells were evenly distributed and grew along the scaffold, and the long axes of most cells were consistent with the direction of the collagen scaffold at day 21 (Fig. 2H–J). A substantial formation of interconnected cellular networks could be observed in the LOCS+NT3+NSC-TrkC group (Fig. S1G). To a certain extent, these experimental results confirmed that the CBD-NT3-modified LOCS promoted the survival and proliferation of iPS-NSCs-TrkC cells, and the effect was significantly better than that of the other two groups.

3.3. CBD-NT3-modified LOCS and TrkC-modified iPSC-derived NSCs constructs a functional neural network

To explore whether the combination of iPS-NSCs-TrkC and LOCS-NT3 could promote a trend of neural differentiation of NSCs, we used immunofluorescence to detect markers associated with neural differentiation and the extracellular matrix after 3D culturing for 21 days in vitro. The cholinergic neuronal marker ChAT and the glutamatergic neuronal marker VGLUT1 were expressed in the LOCS+NT3+NSC-TrkC group. Its fluorescence intensity was higher than that in the LOCS+NT3+NSC and LOCS+NSC-TrkC groups (Fig. 3A–B). The mature neuron marker MAP2 was also highly expressed in the LOCS+NT3+NSC-TrkC group (Fig. 3C). This demonstrates the potential of TrkC-modified iPSC-derived NSCs to differentiate into excitatory neurons in CBD-NT3-modified LOCS in vitro. To further verify the propensity for synapse formation, we detected the synaptophysin marker SYN and postsynaptic density marker PSD95. In the LOCS+NT3+NSC-TrkC group, we found more regions where SYN was adjacent to PSD95 (Fig. 3D), indicating that the LOCS+NT3+NSC-TrkC group had higher potential to form synapses during 3D culture in vitro. Positive staining for GFAP was observed in all groups, indicating that under in vitro cultivation conditions, NSCs still possess a certain capacity for differentiation into astrocytes. The proportion of astrocytic differentiation in the LOCS+NT3+NSC-TrkC group, however, appears to be relatively lower compared to other groups (Fig. 3E).

Previous studies [14,30] and section 3.2 have confirmed LOCS has good biocompatibility, which can provide a good environment for cell growth. To further validate the interaction between the cells and LOCS during binding, we used immunofluorescence to detect laminin and integrin β1. The LOCS+NT3+NSC-TrkC group demonstrated a superior fluorescence intensity of laminin, indicating that the iPS-NSCs-TrkC may secrete more extracellular matrix or factors to shape the environment in vitro. Additionally, the expression of integrin β1-positive cells was also superior in this group (Fig. 3F). Therefore, we speculate that iPS-NSCs-TrkC and CBD-NT3-modified LOCS were not simply combined
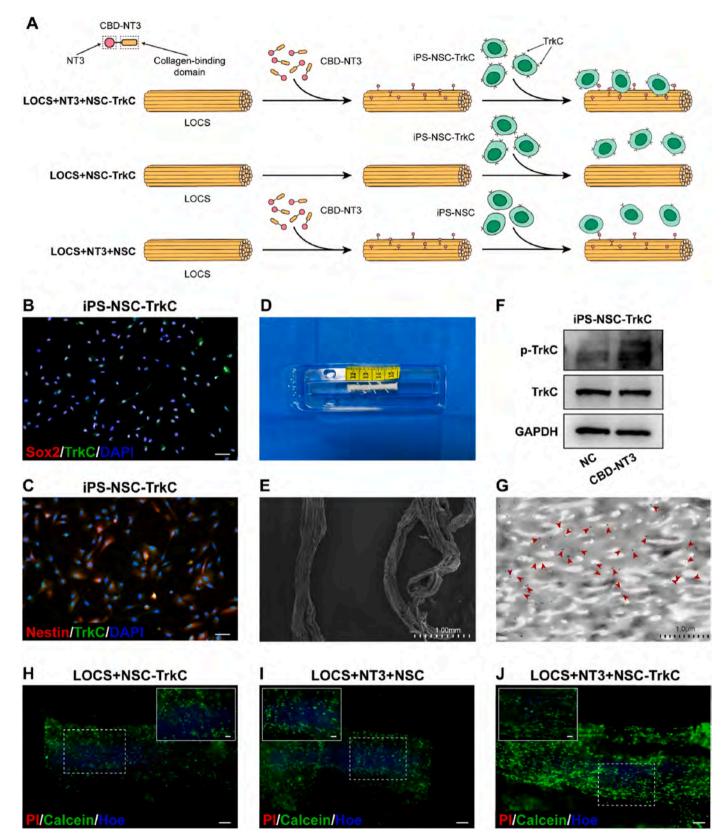
Fig. 2. Construction of functional neural network tissue based on iPSCs-NSCs and LOCS. (A) Flowchart of functional neural network tissue construction. (B) The expression of Sox2 and TrkC in iPSC-derived NSCs. (C) The expression of Nestin and TrkC in iPSC-derived NSCs. (D) Morphology of LOCS. (E) Morphology of LOCS observed by SEM. (F) Western Blot showing the differential phosphorylation level of TrkC between the NC group and CBD-NT3 treated group. (G) The combination of CBD-NT3 and the LOCS (nanogold secondary antibodies were indicated by red arrows). (H–J) Calcein-AM/PI staining to determine the survival status of the cells on the scaffolds of each group at day 21. (Scale bars: 100 μm in B-C, 200 μm in H-J, 100 μm in high-power fields).
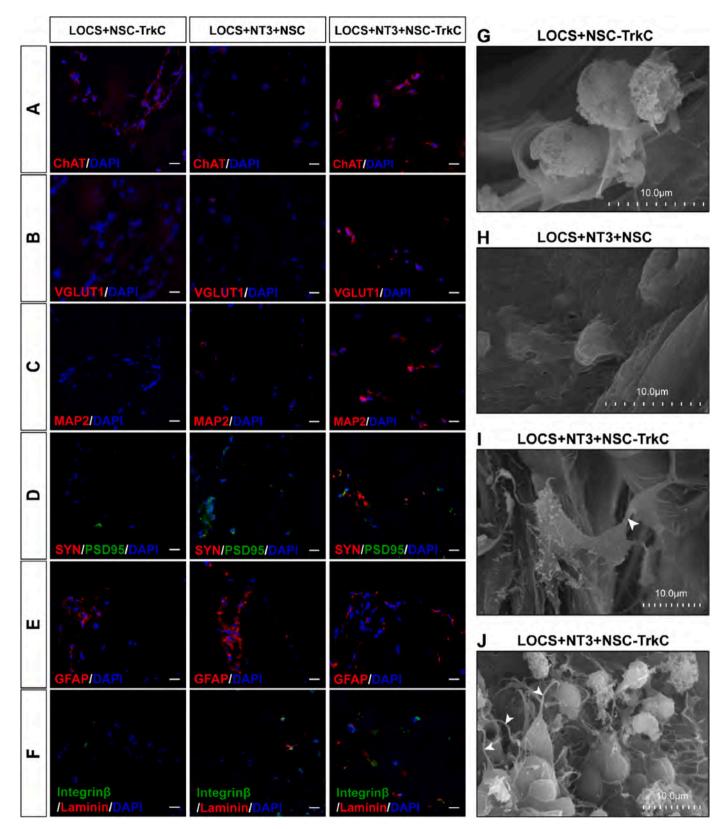
Fig. 3. CBD-NT3-modified LOCS and TrkC-modified iPSC-derived NSCs constructs a functional neural network tissue. (A–B) The expression of cholinergic neuron marker ChAT and glutaminergic neuron marker VGLUT1 in each group in vitro. (C) The expression of mature neuron marker MAP2 in each group in vitro. (D) Synapse formation was determined by immunofluorescence detection of SYN- and PSD95-positive cells. (E) The expression of astrocyte marker GFAP in each group in vitro. (F) The deposition of laminin and the expression of integrin β1-positive cells reflect the interaction between the cells and LOCS (G-J) The cells in each group were also significantly different in morphology, as observed using SEM. Cells made contact with each other through axon-like protrusions, forming a network structure similar to that of neural links (White arrows indicate axon-like protrusions). (Scale bars: 20 μm in A-F).

during 3D culture in vitro. The iPS-NSCs-TrkC reshaped CBD-NT3-modified LOCS by secreting extracellular matrix such as laminin, and the reshaped scaffold further promoted the growth of integrin β1-positive cells. We assume that iPS-NSCs-TrkC and CBD-NT3-modified LOCS can form a self-organized network that may provide long-term maintenance of neural differentiation capacity in vitro.

The cells on each scaffold were also significantly different in morphology, as observed using SEM. In the LOCS+NSC-TrkC and LOCS+NT3+NSC groups, most cells remained spherical, and there were no obvious morphological features of further differentiation (Fig. 3G–H). However, in the LOCS+NT3+NSC-TrkC group, we observed that the cells had differentiated and axon-like protrusions appeared on the cell surface (Fig. 3I). Cells made contact with each other through these processes, forming a network structure similar to that of neural links (Fig. 3J).

Through detailed analyses on 3D cultured tissues in vitro, we showed that TrkC-modified iPSC-derived NSCs and CBD-NT3-modified LOCS can be used to construct a self-organized functional neural network tissue.

3.4. RNA sequencing reveals altered cellular gene expression profiles of iPSC-NSCs-TrkC in the functional neural network tissue

To further identify the gene expression changes in iPS-NSCs-TrkC in 3D cultured functional neural network tissue, we used TRIzol to elute the cells from the scaffold and extracted total RNA for RNA sequencing. Total RNA was extracted from adherent cells as a control (Fig. 4A). Differentially expressed genes (DEGs) were identified using |log2FC| > 1.5 and P value < 0.05 as the criterion. We identified 5684 DEGs, of which 2781 were down-regulated and 2903 were up-regulated (Fig. 4B). We further searched for DEGs associated with neural differentiation. The expression of *SYN1*, *SYN3* and *PSD95* (*DLG4*) in the LOCS+NT3+NSC-TrkC group was significantly higher than NSC-TrkC group, confirming an increased level of axonogenesis and synaptogenesis in the neural network tissue. The elevated expressions of *ChAT*, *VGLUT1* (*SLC17A7*), and *MAP2* indicated the activation of glutamate transport, neuromuscular synaptic transmission, and neurogenesis (Fig. 4C).

We then conducted a functional pathway enrichment analysis using the Gene Ontology (GO) database. In the biological process function category, DEGs were mainly enriched for pathways of extracellular matrix organization, axonogenesis, positive regulation of neurogenesis and cell adhesion, regulation of membrane potential, and synapse organization. In the molecular function category, we observed enrichment in ion channel activity, signaling receptor activator activity and receptor ligand activity. For the enrichment of cellular component category, we identified the synaptic membrane, cell-cell junction, and collagen-containing extracellular matrix pathways (Fig. 4D).

We used GSVA to detail the differences in functional pathways. GSVA analysis showed that iPS-NSCs-TrkC from functional neural network tissue had significantly higher expression of axons, neurons, synapses, neurotransmitters, and myelin-related gene sets than that of adherent cultured cells. The heatmap shows the specific pathway names and gene expression trends for each gene set (Fig. 4E).

RNA sequencing revealed the effect of 3D culture with CBD-NT3-modified LOCS on the cell gene expression profile. These analyses strongly demonstrate the activation of axonogenesis, neurogenesis, synaptogenesis, extracellular matrix organization, and membrane potential in functional neural network tissues.

3.5. Functional neural network tissue transplantation improvs microenvironment of SCI area

Based on the experimental groups described in Section 2.6, we constructed complete transection SCI models to study the effects of functional neural network tissue on SCI in vivo (Fig. S2A). The SCI area

specimens showed no obvious adhesion to the surrounding tissues in the LOCS+NT3+NSC-TrkC group. Compared with the other groups (Figs. S2B–E), the LOCS+NT3+NSC-TrkC group spinal cord specimens showed superior coherence and no obvious atrophy (Fig. S2F). We then used immunofluorescence to detect GFAP-positive cells in the spinal cord of each group. The GFAP-positive cells demonstrated the extent of the SCI area, the SCI areas in the groups with LOCS or cell transplantation were maintained at approximately 3 mm, whereas the blank group showed more obvious atrophy (Fig. 5A–E). Moreover, we found GFAP-positive cells in the SCI area of the LOCS+NT3+NSC-TrkC group, confirming astrocyte regeneration (Fig. 5E).

To observe the survival of the transplanted cells in the SCI area of the rats, we measured HNA expression. Because we used human iPSC-derived NSCs to construct transplanted tissues, the cells were all HNA-positive and were distinguished from the host rat-derived cells. Fewer transplanted cells survived in the LOCS+NSC-TrkC and LOCS+NT3+NSC groups (Fig. 5F–G). However, in the LOCS+NT3+NSC-TrkC group, HNA-positive cells were widely distributed in the SCI area and migrated into normal tissues on both sides of the host spinal cord. This confirmed that the cells successfully survived, proliferated after transplantation, and integrated with the host cells (Fig. 5H).

We measured the expressions of CD68 and NG2 to determine inflammation and scar formation in the SCI area of each group. Compared with the blank group, fewer CD68 positive cells were detected (Fig. 5I-M), and almost no NG2 expression was observed in the LOCS+NT3+NSC-TrkC group (Fig. 5N-R). This indicates that functional neural network tissue transplantation reduced the accumulation of macrophages and deposition of chondroitin sulfate proteoglycans (CSPG) in the SCI area, which could further inhibit inflammation and reduce scar formation. In the LOCS+NT3+NSC-TrkC group, we also found that the level of laminin deposition significantly increased and additional integrin β1-positive cells gathered in this region (Fig. 5S-W). This demonstrates that functional neural network tissue transplantation can substantially improve the microenvironment of the SCI area and promote extracellular matrix remodeling.

3.6. Functional neural network tissue transplantation promotes the regeneration of neurons in SCI area

In the LOCS+NT3+NSC-TrkC group, more Tuj-1 positive cells with much wider distribution were found than in the other control groups (Fig. 6A–B and Figs. S3A–C). Positive cells were observed throughout the lesion at some locations. We quantified the fluorescence intensity of Tuj-1 and GFAP in the spinal cord injury area of the same specimen. Then we calculated the ratio of fluorescence intensity to the number of cells as the relative fluorescence intensity and performed statistical analysis. The LOCS+NT3+NSC-TrkC group exhibited a higher ratio of Tuj-1 to GFAP positive cells (Fig. S4). This showed that functional neural network tissue increasingly promoted the differentiation of cells into neurons in vivo. To clarify the recovery of descending neurons in the SCI area, we determined the distribution of 5-HT positive nerve fibers. The 5-HT positive nerve fibers in the LOCS+NT3+NSC-TrkC group were almost ubiquitous throughout the SCI area, which was significantly better than those in the other control groups. We also found a large number of 5-HT positive fibers in the rostral and caudal regions of the junction between the transplanted area and the host spinal cord and the center of the SCI area (Fig. 6C–D and Figs. S3D–F), demonstrating that the functional neural network tissue implanted into the SCI area could establish neural links between the injured area and the host's spinal cord and remodel the descending neuron function. ChAT and VGLUT1 were also more highly expressed in the LOCS+NT3+NSC-TrkC group, which showed that the functional neural network tissue was superior in promoting the regeneration of excitatory neurons (Fig. 6E–H and Figs. S5A–F). In addition, according to the immunofluorescence results of MBP, the neural network tissue promoted myelin regeneration in the
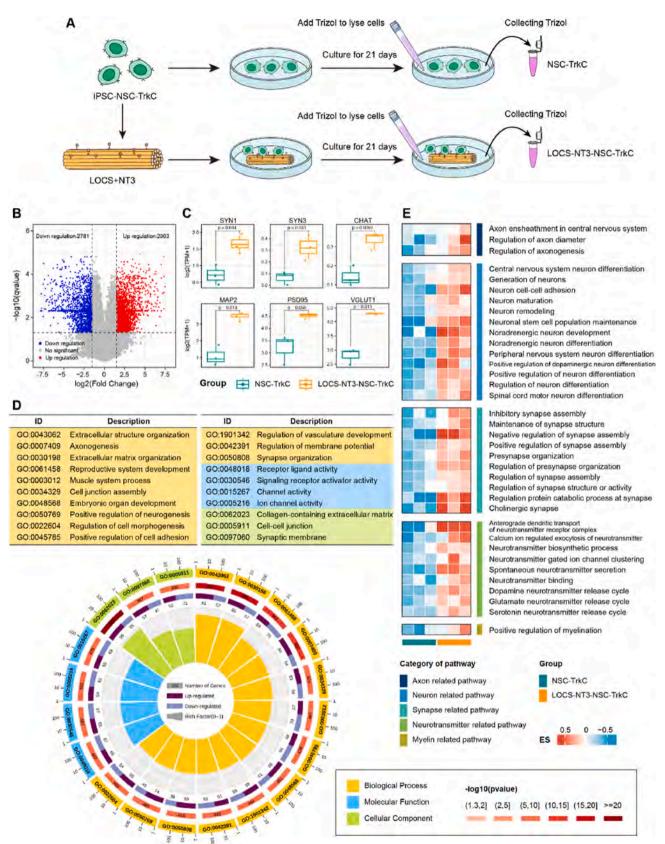
Fig. 4. RNA sequencing reveals altered cellular gene expression profiles of iPSC-NSCs-TrkC in the functional neural network tissue. (A) Flowchart of RNA sequencing. (B) Volcano plot of all DEGs. (C) The expression of *SYN1*, *SYN3* and *PSD95* (*DLG4*) in the LOCS+NT3+NSC-TrkC group was significantly higher than NSC-TrkC group. (D) GO enrichment analysis of DEGs. (E) Heatmap based on GSVA analysis of axons, neurons, synapses, neurotransmitters, and myelin-related gene sets.
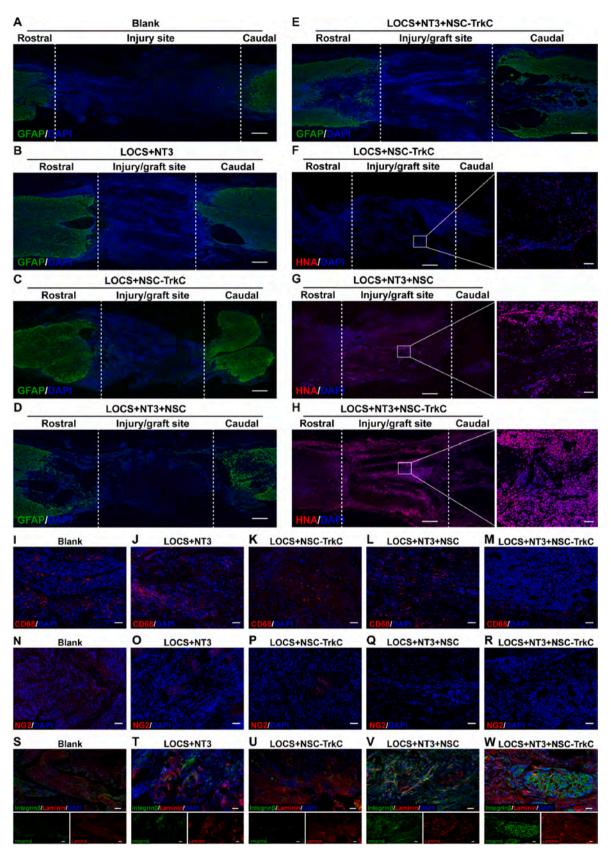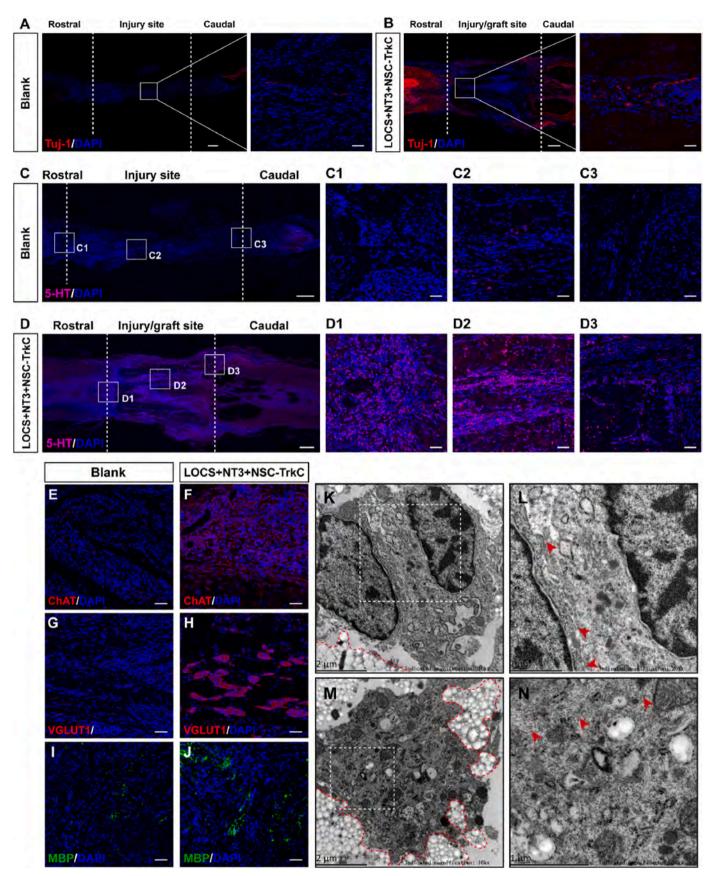
Fig. 5. Functional neural network tissue transplantation improvs microenvironment of SCI area. (A–E) GFAP-positive cells demonstrated the extent of the SCI area and astrocyte regeneration in each group. (F-H) HNA-positive cells demonstrated the survival of the transplanted cells in the SCI area of the rats in each group. (I–M) CD68-positive cells determined inflammation in SCI area of each group. (N–R) NG2 determined scar formation in SCI area of each group. (S-W) The deposition of laminin and the expression of integrin β1-positive cells reflected functional neural network tissue transplantation can substantially improve the microenvironment of the SCI area and promote extracellular matrix remodeling. (Scale bars: 500 μm in A-H, 50 μm in I-W and all high-power fields).

(caption on next page)

Fig. 6. Functional neural network tissue transplantation promotes the regeneration of neurons in SCI area. (A–B) Tuj-1 positive cells reflected functional neural network tissue increasingly promoted the differentiation of cells into neurons in vivo. (C–D) 5-HT positive fibers were found in the rostral and caudal regions of the junction between the transplanted area and the host spinal cord and the center of the SCI area in the LOCS+NT3+NSC-TrkC group, which was significantly better than those in the other control groups. (E–J) The expression of cholinergic neuron marker ChAT, glutaminergic neuron marker VGLUT1 and MBP showed that the functional neural network tissue was superior in promoting the regeneration of excitatory neurons and myelin. (K–L) Neurons with normal morphology and structure were found in the center of the SCI area in the LOCS+NT3+NSC-TrkC group, and connection structures of the two neurons were observed (connection structures were indicated by red arrows, LOCS were indicated by red dotted line). (M–N) Organelle structures and neurofilaments were also observed in the by TEM (neurofilaments were indicated by red arrows, LOCS were indicated by red dotted line). (Scale bars: 500 μm in A-D, 50 μm in E-J and all high-power fields).

SCI area (Fig. 6I–J and Figs. S5G–I).

To determine whether synapse formation occurred in the SCI area in vivo, we used immunofluorescence to detect SYN and PSD95 expression levels. In the LOCS+NT3+NSC-TrkC group, more SYN-positive cells were detected, and there were more SYN and PSD95 positive regions adjacent or co-expressed than in the other control groups (Fig. S6). This suggests that additional presynaptic and postsynaptic membrane structures could be formed after transplanting functional neural network tissue into the SCI area, which may have the potential to form synaptic structures.

We further observed the neurons in the SCI area using TEM. Neurons with normal morphology and structure were found in the center of the SCI area in the LOCS+NT3+NSC-TrkC group, and connection structures of the two neurons were observed (Fig. 6K-L). The neurons were tightly attached to the LOCS, grew and extended around the LOCS (Fig. 6M). Organelle structures and neurofilaments were also observed in the neurons, thereby confirming that they contain normal neuronal functions (Fig. 6N). In contrast, in the other control groups, fibroblasts or structurally abnormal neurons were mainly observed by TEM (Fig. S7).

In this section, we demonstrated that functional neural network tissue transplantation effectively promotes the regeneration of excitatory neurons and formation of synaptic structures in the SCI area. The transplanted tissue established neural connections with the rostral and caudal parts of the injured area and acted as a relay station for the neural circuits.

3.7. RNA sequencing reveals gene expression profile changes in SCI area

To investigate the mechanism of SCI recovery after functional neural network tissue implantation, we used RNA sequencing to study the gene expression profile changes in the SCI area. We also used TPM to standardize the sequencing data, with $|log2FC| > 1$ and P value < 0.05 as the criteria for DEGs. Compared to the blank group, 1234 DEGs were filtered in the LOCS+NT3+NSC-TrkC group, including 600 up-regulated and 634 down-regulated genes (Fig. 7A). We used the GO database to analyze functional pathway enrichment based on the DEGs (Fig. 7E). In the molecular function category, DEGs were mainly enriched for signaling receptor activator activity, receptor ligand activity, ion channel activity and cation channel activity. The biological process category was enriched for second-messenger-mediated signaling, lipid localization and transport, regulation of cytosolic calcium ion concentration, and carboxylic acid and organic acid transport. In the cellular component category, we observed an enrichment of the receptor and transporter complex pathways. This reflects the activation of material transport, intercellular message conduction, and ion channel capacity in the SCI area after functional neural network tissue implantation.

We further analyzed the functional differences in axons, neurons, synapses, neurotransmitters, and myelin-related pathways using GSVA (Fig. 7F). The heatmap revealed a significant positive regulation of axon formation, extension and regulation, neuron maturation, migration and recognition, synaptic formation, GABA and glutamate neuronal signal transduction, myelin formation, and other functions in the SCI area after functional neural network tissue implantation.

A protein-protein interaction network analysis was also performed based on these DEGs. We identified some key molecules such as Rsad2, Ttk, Slc17a7, Alb, Erbb4, Fgf21, and Wnt9b (Fig. S8A). This suggests that functional neural network tissue may have affected the recovery of

SCI by regulating the MAPK, PI3K-Akt, Wnt, calcium, GABAergic, and glutamatergic synapse pathways.

RNA sequencing has revealed the mechanism of functional neural network tissue transplantation in promoting spinal cord function recovery from multiple perspectives. This confirmed that the tissue promoted the regeneration of excitatory and inhibitory neurons and formation of synaptic structures, axons, and myelin.

3.8. Metabolomics analysis reveals pathophysiological differences in recovery process of SCI area

We screened 50 different small-molecule metabolites with a filter of $|logFC| > 0$ and a P-value of <0.05. Compared with the blank group, there were 8 up-regulated metabolites and 42 down-regulated metabolites in the LOCS+NT3+NSC-TrkC group (Fig. 7B). Among the metabolically different small-molecule metabolites, 38.64 % were lipids and lipid-like molecules, indicating notable difference in lipid metabolism between the two groups (Fig. 7C). Using the Kyoto Encyclopedia of Genes and Genomes (KEGG) database, we found that different small-molecule metabolites were enriched in the ether lipid metabolism, glycerophospholipid metabolism, and neuroactive ligand-receptor interaction pathways (Fig. 7D). The interactive Pathways Explore (iPath) demonstrated the influence of differential metabolites on metabolic pathways. In the LOCS+NT3+NSC-TrkC group, energy metabolism and NADH-NAD$^+$ cycling were more significant (Figs. S8B–D), indicating that the metabolism of the SCI area was high after functional neural network tissue transplantation. These differential metabolites also affected glutamate and tyrosine metabolism, which led to increased GABA and L-Dopa production in the LOCS+NT3+NSC-TrkC group (Figs. S8E–G).

3.9. Functional neural network tissue transplantation could improve SCI rat locomotor function

After feeding the rats for 8 weeks after surgery, hind limb motor function was evaluated using the BBB scale. The rats in LOCS+NT3+NSC-TrkC group (9.25 ± 3.59) had a superior BBB scale compared to other groups, and was statistically different compared with the blank group (1.75 ± 1.39). The BBB scale of the other control groups transplanted with LOCS and NSCs were lower, but were also higher than those of the blank group (Fig. 8A). The results of the inclined grid climbing test confirmed that rats in the LOCS+NT3+NSC-TrkC group exhibited noticeable voluntary movements in the hind limbs, demonstrating a significant recovery in both motor function and coordination (Fig. S9, Video S1-4). The daily activities of these two groups of rats also reflected the difference in the recovery of hindlimb motor function (Video S5-6).

Supplementary video related to this article can be found at https://doi.org/10.1016/j.bioactmat.2024.01.012

We used an evoked potential apparatus to record the cortical motor-evoked potentials (CMEPs) of rats after transplantation. The CMEPs were recorded in all groups (Fig. 8B). We calculated the latency and amplitude of the CMEP to reflect the speed and amplitude of the cortical signal passing through the SCI area. In all the experimental groups treated with transplantation, the latencies were shorter than those in the blank group. The latency of the LOCS+NT3+NSC-TrkC group (4.18 ± 0.13 ms) was the shortest, and was statistically significant compared
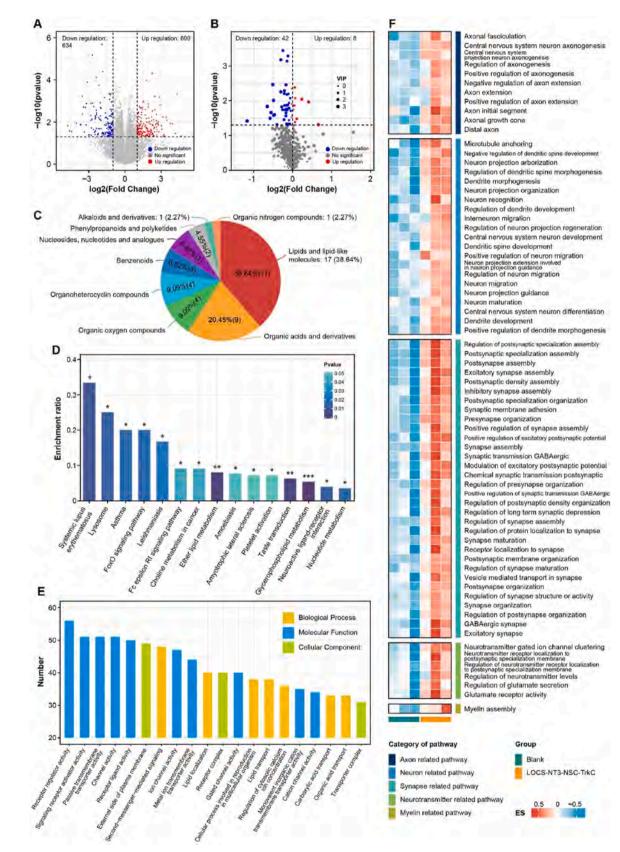
Fig. 7. RNA sequencing and metabolomics analysis reveal gene expression profile changes and pathophysiological differences in injured area. (A) Volcano plot of all DEGs. (B) Volcano plot of all different small-molecule metabolites. (C) Categories of different small-molecule metabolites. (D) KEGG enrichment analysis of different small-molecule metabolites. (E) GO enrichment analysis of DEGs. (F) Heatmap based on GSVA analysis of axons, neurons, synapses, neurotransmitters, and myelin-related gene sets. (*: p < 0.05; **: p < 0.01; ***: p < 0.001).
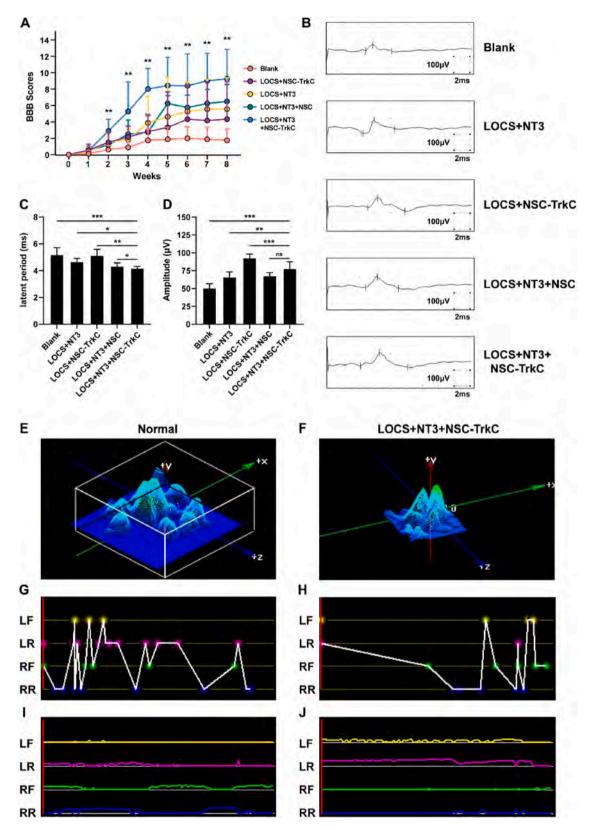
Fig. 8. Functional neural network tissue transplantation could improve SCI rat locomotor function. (A) The rats in LOCS+NT3+NSC-TrkC group had a superior BBB scale compared to other groups, and was statistically different compared with the blank group. (B) The representative CMEPs results of each group were recorded. (C) The latency of the LOCS+NT3+NSC-TrkC group was the shortest, and was statistically significant compared with other groups. (D) The statistics analysis of amplitude showed a significant difference between the transplantation-treated and blank groups. (E–F) Compared with the normal rats, the hind claw weight-bearing in the LOCS+NT3+NSC-TrkC group were mainly concentrated in the palm and great toe. (G–H) The step sequence analysis detected discontinuous coordinated hindlimb movements in the LOCS+NT3+NSC-TrkC group. (I–J) The dwell intensity curves confirmed that both hind limbs of the rats successfully bore weight and moved during walking in the LOCS+NT3+NSC-TrkC group. (*: $p < 0.05$; **: $p < 0.01$; ***: $p < 0.001$).

with other groups (Fig. 8C). The statistics analysis of amplitude also showed a significant difference between the transplantation-treated and blank group (Fig. 8D).

From the animal gait analysis, in normal rats, weight bearing of the left hind claw was dominated by the palms and toes (Fig. 8E). The step sequence and dwell intensity curves are shown in Fig. 8G and I, respectively. In our experiment, only the recovery of the rats in the LOCS+NT3+NSC-TrkC group met the animal gait analysis requirement. Compared with the normal rats, the hind claw weight-bearing in the LOCS+NT3+NSC-TrkC group were mainly concentrated in the palm and great toe (Fig. 8F). Step sequence analysis detected discontinuous coordinated hindlimb movements (Fig. 8H). The dwell intensity curves confirmed that both hind limbs of the rats in the LOCS+NT3+NSC-TrkC group successfully bore weight and moved during walking (Fig. 8J).

These results confirm that the transplantation of LOCS scaffolds can promote the recovery of hind limb function in SCI rats. Functional neural network tissues based on TrkC-modified iPSC-derived NSCs and CBD-NT3-modified LOCS can significantly further improve locomotor function.

4. Discussion

iPSCs are pluripotent self-renewing cells that are reprogrammed from terminally differentiated somatic cells by introducing specific genes or molecules [21]. iPSCs have been widely used in the research fields of Parkinson's disease, Alzheimer's disease, and other nervous system diseases [31,32]. Because of their ability to differentiate into NSCs, it is believed that they can effectively solve the problem of obtaining individualized NSCs in SCI repair [19].

Several groups have used iPSC-derived NSCs to treat SCI. Fujimoto et al. showed that the therapeutic potential of human iPSC-NSCs in a mouse model of SCI was comparable to that of NSCs from the human fetal spinal cord [33]. Other groups have also found that iPSC-NSC transplantation in SCI areas can promote myelination and axon regeneration, reduce inflammation, and improve hind limb function to some extent [34,35]. In addition, recent animal transplantation results have confirmed that iPSC-derived cells are safe for transplantation during SCI treatment [36,37]. Some teams have also combined iPSC-NSCs with scaffolds for SCI repair. Although integration between the implant and host has been observed in experiments, no significant recovery of motor function has been observed [38,39]. The repair of SCI by exogenous cell transplantation generally faces many problems, such as migration and spreading of transplanted cells by cerebrospinal fluid washing, low cell survival ratio, and inability of axon directional growth [40]. To combine exogenous cells with scaffold materials and transplant them into the SCI area, implants may also inhibit functional recovery owing to problems such as space-occupying effects. Collagen is often used for tissue regeneration in tissue engineering. LOCS obtained by designing and modifying collagen are biocompatible materials with an ordered and oriented spatial structure. Previous studies have shown that implantation of LOCS in rats, beagles, and macaques SCI models can promote the accumulation of stem cells in the SCI area, inhibit the formation of glial scars, provide support for neuronal growth and axon extension in a directed manner, and improve animal limb function, thereby suggesting that LOCS have SCI regeneration and repair abilities [10,13,14]. Therefore, we designed this functional neural network tissue in this study hoping to fully exploit the characteristics and advantages of LOCS and iPSCs. This approach can effectively solve the problem of the transplanted NSCs source, as well as enable the transplanted cells to effectively influence the SCI area through the support of LOCS and further improve the repair efficacy of SCI.

NT3 binds to TrkC expressed on the cell surface to activate the NT3/TrkC signaling pathway and promotes synaptic formation and neural circuit development [41]. Studies have shown that NT3 single neurotrophic factor therapy can improve the microenvironment after SCI and promote endogenous repair [42]. Our previous studies, as well as those

of other groups, have confirmed that the transplantation of scaffold materials containing NT3 can inhibit scar formation and promote axon regeneration and nerve circuit reconstruction [13,43]. Zeng et al. also used an NT3 binding fibrin scaffold combined with rat brain-derived NSCs overexpressing TrkC to achieve promising results in a rat SCI model [44]. These results confirmed that NT3 improved the treatment efficacy of SCI. Therefore, CBD-NT3 was constructed to enhance the binding ability of NT3 to LOCS and ensure that additional NT3 would remain in the transplanted area and continue to exert influence. We also overexpressed TrkC in transplanted iPSC-NSCs to strengthen the connection between cells and LOCS as well as enable NT3 to fully act on the transplanted cells.

We verified the biological function of this functional neural network tissue based on CBD-NT3-modified LOCS and TrkC-modified iPSC-derived NSCs in vitro. Calcein-AM staining and immunofluorescence confirmed that iPSC-NSCs-TrkC in the functional neural network tissue proliferated, differentiated, and grew along the direction of the LOCS, which represented a significantly better result than other control groups. We also found that these cells differentiated into multiple excitatory neurons and formed synapses when cultured in vitro. The extensive deposition of laminin in the tissues and the expression of integrin β1-positive cells also indicated that this functional neural network tissue was not a simple binding of LOCS and the cells. iPSC-NSCs-TrkC remodeled LOCS-NT3 by secreting more extracellular matrix, and this remodeling also improved the extracellular microenvironment and promoted the further growth of integrin β positive cells. This suggests that the components within the tissue can influence and optimize each other, which also explains the formation of a self-organized functional neural network tissue.

In the in vivo experiments, following implantation of the network tissue, the spinal cord in the injured area was coherent, adhesion was reduced, and no obvious glial scar formation was observed. Immunofluorescence also confirmed that CD68 positive cells and CSPG-positive areas were significantly reduced compared to those in the control groups. We also further detected the expression of laminin and integrin β1-positive cells in the SCI area. This also indicates that the functional neural network tissue produced a better extracellular matrix remodeling in the SCI area than the other controls. Laminin is an important extracellular matrix protein that promotes axon growth both in vivo and in vitro [45]. A laminin integrin-dependent mechanism can regulate the inhibitory effect of CSPG on axonal growth and promote axon regeneration [46,47]. We believe that the extracellular matrix remodeling of the SCI area by functional neural network tissue is one of the mechanisms that can promote nerve regeneration in the SCI area and form a relay station for neural circuits.

RNA sequencing validated the immunofluorescence results in terms of gene expression profiles. Functional enrichment analyses, such as GSVA, were also performed based on sequencing data to more effectively demonstrate the effects of functional neural network tissues on biological functions, such as axons, neurons, synapses, neurotransmitters, and cell adhesion in vitro and in vivo. We also screened the molecules most closely related to the process of SCI repair in the transplanted tissue through protein-protein interaction networks. ErbB4 participates in regulating the PI3K/AKT and MAPK/ERK pathways [48], and is closely related to sensory nerve conduction. NRG1-ErbB4 signaling also regulates the dynamic activity of tyrosine kinases and influences glutamatergic transmission [49]. FGF21 is closely associated with energy metabolism and exerts a neuroprotective influence by regulating neuroinflammation and oxidative-stress responses [50]. FGF21 is also associated with PI3K/AKT and MAPK pathways. Metabolomic analysis also revealed metabolic changes in the SCI area after implantation of the functional neural network tissue, confirming its influence on energy metabolism and neurotransmitter formation in the SCI area. We believe that the application of multi-omics analysis in SCI can evaluate the therapeutic effect of SCI as well as analyze the potential mechanism of SCI repair at multiple levels. Moreover, this analysis can

more effectively identify key molecules that affect SCI regeneration and provide new ideas for subsequent study.

Although LOCS offer numerous advantages in the treatment of SCI, there is still potential for further improvement to enhance SCI repair. One approach to achieve this is by improving the adhesion of cells with the scaffold through covalent conjugation. Liu et al. conducted a study where metabolic azido-labelled human neural progenitor cells were conjugated on dibenzocyclooctyne-modified LOCS. They found that this significantly enhanced cell adhesion, spreading, and differentiation compared to noncovalent adhesion [51]. In addition, the components of the scaffold implanted into SCI sites play a crucial role in the efficacy of therapy. Chen et al. developed aligned decellularized spinal cord fibers (A-DSCF) to promote axonal regeneration and remyelination after SCI. When A-DSCF was loaded with neural progenitor cells, it led to improved survival, maturation, axon regeneration, and motor function in SCI rats [52]. It emphasizes the importance of using structurally and compositionally biomimetic scaffolds to load exogenous stem cells for SCI repair in the future.

In this study, we attempted to construct a functional neural network tissue using human iPS-NSCs as seed cells based on the interaction of receptors and ligands for the first time. It effectively provides a solution for individualized acquisition of exogenous NSCs, and expands the application prospect of iPS-NSCs and LOCS in SCI repair research, which presents a new idea of biomaterial design for SCI regeneration and repair.

5. Conclusions

In this study, we constructed a functional neural network tissue based on TrkC-modified iPSC-derived NSCs and CBD-NT3-modified LOCS for the repair and regeneration of SCI. After transplantation into the SCI area, the tissue effectively improved the microenvironment, enhanced remodeling of the extracellular matrix, and promoted the regeneration of neurons and synapse formation. This tissue can be used as a relay station to rebuild neural circuits and effectively improve the motor function of the hind limbs. This study solved the difficult problem of determining a cell source for transplantation in SCI treatment as well as further confirmed the effectiveness of LOCS and iPSCs for SCI repair and regeneration. This study also demonstrates the feasibility of using biomaterials based on the interaction between receptors and ligands for SCI research.

Ethical statement

All animal experiments were conducted in compliance with the Chinese Ministry of Public Health Guide for Animal Ethics and Welfare. This study was approved by the Ethics Committee of the Xiangya Hospital of Central South University and the Department of Laboratory Animals of Central South University. Ethics No. CSU-2022-01-0099.

CRediT authorship contribution statement

Zhaoping Wu: Data curation, Formal analysis, Methodology, Writing – original draft. **Yi Zhou:** Data curation, Formal analysis, Methodology, Writing – original draft. **Xianglin Hou:** Methodology. **Weidong Liu:** Writing – review & editing. **Wen Yin:** Methodology. **Lei Wang:** Writing – review & editing. **Yudong Cao:** Methodology. **Zhipeng Jiang:** Methodology. **Youwei Guo:** Methodology. **Quan Chen:** Data curation. **Wen Xie:** Methodology. **Ziqiang Wang:** Data curation. **Ning Shi:** Methodology. **Yujun Liu:** Methodology. **Xiang Gao:** Supervision. **Longlong Luo:** Supervision. **Jianwu Dai:** Funding acquisition, Resources, Supervision. **Caiping Ren:** Conceptualization, Funding acquisition, Supervision, Writing – review & editing. **Xingjun Jiang:** Conceptualization, Funding acquisition, Supervision, Writing – review & editing.

Declaration of competing interest

The authors declare that this study did not involve any commercial funding or potential conflicts of interest that could have influenced the results.

Appendix A. Supplementary data

Supplementary data to this article can be found online at https://doi.org/10.1016/j.bioactmat.2024.01.012.

References

[1] C.S. Ahuja, J.R. Wilson, S. Nori, M.R.N. Kotter, C. Druschel, A. Curt, M.G. Fehlings, Traumatic spinal cord injury, Nat. Rev. Dis. Prim. 3 (2017) 17018, https://doi.org/10.1038/nrdp.2017.18.

[2] M.A. Anderson, J.W. Squair, M. Gautier, T.H. Hutson, C. Kathe, Q. Barraud, J. Bloch, G. Courtine, Natural and targeted circuit reorganization after spinal cord injury, Nat. Neurosci. 25 (12) (2022) 1584–1596, https://doi.org/10.1038/s41593-022-01196-1.

[3] J.W. McDonald, C. Sadowsky, Spinal-cord injury, Lancet 359 (9304) (2002) 417–425, https://doi.org/10.1016/S0140-6736(02)07603-1.

[4] A. Anjum, M.D. Yazid, M. Fauzi Daud, J. Idris, A.M.H. Ng, A. Selvi Naicker, O.H. R. Ismail, R.K. Athi Kumar, Y. Lokanathan, Spinal cord injury: pathophysiology, multimolecular interactions, and underlying recovery mechanisms, Int. J. Mol. Sci. 21 (20) (2020) 7533, https://doi.org/10.3390/ijms21207533.

[5] A. Alizadeh, S.M. Dyck, S. Karimi-Abdolrezaee, Traumatic spinal cord injury: an overview of pathophysiology, models and acute injury mechanisms, Front. Neurol. 10 (2019) 282, https://doi.org/10.3389/fneur.2019.00282.

[6] E.A. Kiyotake, M.D. Martin, M.S. Detamore, Regenerative rehabilitation with conductive biomaterials for spinal cord injury, Acta Biomater. 139 (2022) 43–64, https://doi.org/10.1016/j.actbio.2020.12.021.

[7] Q. Han, W. Sun, H. Lin, W. Zhao, Y. Gao, Y. Zhao, B. Chen, Z. Xiao, W. Hu, Y. Li, B. Yang, J. Dai, Linear ordered collagen scaffolds loaded with collagen-binding brain-derived neurotrophic factor improve the recovery of spinal cord injury in rats, Tissue Eng. 15 (10) (2009) 2927–2935, https://doi.org/10.1016/j.actbio.2020.12.021.

[8] H. Lin, B. Chen, B. Wang, Y. Zhao, W. Sun, J. Dai, Novel nerve guidance material prepared from bovine aponeurosis, J. Biomed. Mater. Res. 79 (3) (2006) 591–598, https://doi.org/10.1002/jbm.a.30862.

[9] Q. Han, W. Jin, Z. Xiao, H. Ni, J. Wang, J. Kong, J. Wu, W. Liang, L. Chen, Y. Zhao, B. Chen, J. Dai, The promotion of neural regeneration in an extreme rat spinal cord injury model using a collagen scaffold containing a collagen binding neuroprotective protein and an EGFR neutralizing antibody, Biomaterials 31 (35) (2010) 9212–9220, https://doi.org/10.1016/j.biomaterials.2010.08.040.

[10] W. Yin, X. Li, Y. Zhao, J. Tan, S. Wu, Y. Cao, J. Li, H. Zhu, W. Liu, G. Tang, L. Meng, L. Wang, B. Zhu, G. Wang, M. Zhong, X. Liu, D. Xie, B. Chen, C. Ren, Z. Xiao, X. Jiang, J. Dai, Taxol-modified collagen scaffold implantation promotes functional recovery after long-distance spinal cord complete transection in canines, Biomater. Sci. 6 (5) (2018) 1099–1108, https://doi.org/10.1039/c8bm00125a.

[11] D. Liu, X. Li, Z. Xiao, W. Yin, Y. Zhao, J. Tan, B. Chen, X. Jiang, J. Dai, Different functional bio-scaffolds share similar neurological function to promote locomotor recovery of canines with complete spinal cord injury, Biomaterials 214 (2019) 119230, https://doi.org/10.1016/j.biomaterials.2019.119230.

[12] J. Fan, Z. Xiao, H. Zhang, B. Chen, G. Tang, X. Hou, W. Ding, B. Wang, P. Zhang, J. Dai, R. Xu, Linear ordered collagen scaffolds loaded with collagen-binding neurotrophin-3 promote axonal regeneration and partial functional recovery after complete spinal cord transection, J. Neurotrauma 27 (9) (2010) 1671–1683, https://doi.org/10.1089/neu.2010.1281.

[13] S. Han, X. Li, S. Wu, Y. Cao, J. Tan, Y. Zhao, X. Hou, L. Wang, C. Ren, J. Li, X. Hu, Y. Mao, G. Li, B. Li, H. Zhang, J. Han, B. Chen, Z. Xiao, X. Jiang, J. Dai, Pre-clinical evaluation of CBD-NT3 modified collagen scaffolds in completely spinal cord transected non-human primates, J. Neurotrauma 36 (15) (2019) 2316–2324, https://doi.org/10.1089/neu.2018.6078.

[14] W. Yin, W. Xue, H. Zhu, H. Shen, Z. Xiao, S. Wu, Y. Zhao, Y. Cao, J. Tan, J. Li, W. Liu, L. Wang, L. Meng, B. Chen, M. Zhao, X. Jiang, X. Li, C. Ren, J. Dai, Scar tissue removal-activated endogenous neural stem cells aid Taxol-modified collagen scaffolds in repairing chronic long-distance transected spinal cord injury, Biomater. Sci. 9 (13) (2021) 4778–4792, https://doi.org/10.1039/d1bm00449b.

[15] Z. You, X. Gao, X. Kang, W. Yang, T. Xiong, Y. Li, F. Wei, Y. Zhuang, T. Zhang, Y. Sun, H. Shen, J. Dai, Microvascular endothelial cells derived from spinal cord

promote spinal cord injury repair, Bioact. Mater. 29 (2023) 36–49, https://doi.org/10.1016/j.bioactmat.2023.06.019.

[16] C. Jin, Y. Wu, H. Zhang, B. Xu, W. Liu, C. Ji, P. Li, Z. Chen, B. Chen, J. Li, X. Wu, P. Jiang, Y. Hu, Z. Xiao, Y. Zhao, J. Dai, Spinal cord tissue engineering using human primary neural progenitor cells and astrocytes, Bioeng Transl Med 8 (2) (2023) e10448, https://doi.org/10.1002/btm2.10448.

[17] J. Yao, Y. Mu, F.H. Gage, Neural stem cells: mechanisms and modeling, Protein Cell 3 (4) (2012) 251–261, https://doi.org/10.1007/s13238-012-2033-6.

[18] M. Stenudd, H. Sabelstrom, J. Frisen, Role of endogenous neural stem cells in spinal cord injury and repair, JAMA Neurol. 72 (2) (2015) 235–237, https://doi.org/10.1001/jamaneurol.2014.2927.

[19] M. Martin-Lopez, B. Fernandez-Munoz, S. Canovas, Pluripotent stem cells for spinal cord injury repair, Cells 10 (12) (2021) 3334, https://doi.org/10.3390/cells10123334.

[20] K. Takahashi, S. Yamanaka, Induction of pluripotent stem cells from mouse embryonic and adult fibroblast cultures by defined factors, Cell 126 (4) (2006) 663–676, https://doi.org/10.1016/j.cell.2006.07.024.

[21] E.P. Papapetrou, Induced pluripotent stem cells, past and future, Science 353 (6303) (2016) 991–992, https://doi.org/10.1126/science.aai7626.

[22] O. Tsuji, K. Sugai, R. Yamaguchi, S. Tashiro, N. Nagoshi, J. Kohyama, T. Iida, T. Ohkubo, G. Itakura, M. Isoda, M. Shinozaki, K. Fujiyoshi, Y. Kanemura, S. Yamanaka, M. Nakamura, H. Okano, Concise review: laying the groundwork for a first-in-human study of an induced pluripotent stem cell-based intervention for spinal cord injury, Stem Cell. 37 (1) (2019) 6–13, https://doi.org/10.1002/stem.2926.

[23] Y. Naito, A.K. Lee, H. Takahashi, Emerging roles of the neurotrophin receptor TrkC in synapse organization, Neurosci. Res. 116 (2017) 10–17, https://doi.org/10.1016/j.neures.2016.09.009.

[24] B. Tepper, K. Bartkowska, M. Okrasa, M. Ngati, M. Braszak, K. Turlejski, R. Djavadian, Downregulation of TrkC receptors increases dendritic arborization of purkinje cells in the developing cerebellum of the opossum, monodelphis domestica, Front. Neuroanat. 14 (2020) 56, https://doi.org/10.3389/fnana.2020.00056.

[25] S. Li, H. Liu, W. Liu, N. Shi, M. Zhao, S. Wanggou, W. Luo, L. Wang, B. Zhu, X. Zuo, Xie, C. Zhao, Y. Zhou, L. Luo, X. Gao, X. Jiang, C. Ren, ESRG is critical to maintain the cell survival and self-renewal/pluripotency of hPSCs by collaborating with MCM2 to suppress p53 pathway, Int. J. Biol. Sci. 19 (3) (2023) 916–935, https://doi.org/10.7150/ijbs.79095.

[26] Y. Zhao, F. Tang, Z. Xiao, G. Han, N. Wang, N. Yin, B. Chen, X. Jiang, C. Yun, W. Han, C. Zhao, S. Cheng, S. Zhang, J. Dai, Clinical study of NeuroRegen scaffold combined with human mesenchymal stem cells for the repair of chronic complete spinal cord injury, Cell Transplant. 26 (5) (2017) 891–900, https://doi.org/10.3727/096368917X695038.

[27] S. Chen, Y. Zhou, Y. Chen, J. Gu, fastp: an ultra-fast all-in-one FASTQ preprocessor, Bioinformatics 34 (17) (2018) i884–i890, https://doi.org/10.1093/bioinformatics/bty560.

[28] D. Kim, B. Langmead, S.L. Salzberg, HISAT: a fast spliced aligner with low memory requirements, Nat. Methods 12 (4) (2015) 357–360, https://doi.org/10.1038/nmeth.3317.

[29] M. Pertea, G.M. Pertea, C.M. Antonescu, T.C. Chang, J.T. Mendell, S.L. Salzberg, StringTie enables improved reconstruction of a transcriptome from RNA-seq reads, Nat. Biotechnol. 33 (3) (2015) 290–295, https://doi.org/10.1038/nbt.3122.

[30] X. Li, J. Tan, Z. Xiao, Y. Zhao, S. Han, D. Liu, W. Yin, J. Li, J. Li, S. Wanggou, B. Chen, C. Ren, X. Jiang, J. Dai, Transplantation of hUC-MSCs seeded collagen scaffolds reduces scar formation and promotes functional recovery in canines with chronic spinal cord injury, Sci. Rep. 7 (2017) 43559, https://doi.org/10.1038/srep43559.

[31] H. Okano, S. Morimoto, iPSC-based disease modeling and drug discovery in cardinal neurodegenerative disorders, Cell Stem Cell 29 (2) (2022) 189–208, https://doi.org/10.1016/j.stem.2022.01.007.

[32] M. Jin, R. Xu, L. Wang, M.M. Alam, Z. Ma, S. Zhu, A.C. Martini, A. Jadali, M. Bernabucci, P. Xie, K.Y. Kwan, Z.P. Pang, E. Head, Y. Liu, R.P. Hart, P. Jiang, Type-I-interferon signaling drives microglial dysfunction and senescence in human iPSC models of Down syndrome and Alzheimer's disease, Cell Stem Cell 29 (7) (2022) 1135–1153 e8, https://doi.org/10.1016/j.stem.2022.06.007.

[33] Y. Fujimoto, M. Abematsu, A. Falk, K. Tsujimura, T. Sanosaka, B. Juliandi, K. Semi, M. Namihira, S. Komiya, A. Smith, K. Nakashima, Treatment of a mouse model of spinal cord injury by transplantation of human induced pluripotent stem cell-derived long-term self-renewing neuroepithelial-like stem cells, Stem Cell. 30 (6) (2012) 1163–1173, https://doi.org/10.1002/stem.1083.

[34] D. Kong, B. Feng, A.E. Amponsah, J. He, R. Guo, B. Liu, X. Du, X. Liu, S. Zhang, F. Lv, J. Ma, H. Cui, hiPSC-derived NSCs effectively promote the functional recovery of acute spinal cord injury in mice, Stem Cell Res. Ther. 12 (1) (2021) 172, https://doi.org/10.1186/s13287-021-02217-9.

[35] T. Amemori, J. Ruzicka, N. Romanyuk, M. Jhanwar-Uniyal, E. Sykova, P. Jendelova, Comparison of intraspinal and intrathecal implantation of induced pluripotent stem cell-derived neural precursors for the treatment of spinal cord injury in rats, Stem Cell Res. Ther. 6 (2015) 257, https://doi.org/10.1186/s13287-015-0255-2.

[36] L. Chow, S. McGrath, C. de Arruda Saldanha, L.R. Whalen, R. Packer, S. Dow, Generation of neural progenitor cells from canine induced pluripotent stem cells and preliminary safety test in dogs with spontaneous spinal cord injuries, Front. Vet. Sci. 7 (2020) 575938, https://doi.org/10.3389/fvets.2020.575938.

[37] M. Martin-Lopez, E. Gonzalez-Munoz, E. Gomez-Gonzalez, R. Sanchez-Pernaute, J. Marquez-Rivas, B. Fernandez-Munoz, Modeling chronic cervical spinal cord injury in aged rats for cell therapy studies, J. Clin. Neurosci. 94 (2021) 76–85, https://doi.org/10.1016/j.jocn.2021.09.042.

[38] P. Bonilla, J. Hernandez, E. Giraldo, M.A. Gonzalez-Perez, A. Alastrue-Agudo, H. Elkhenany, M.J. Vicent, X. Navarro, M. Edel, V. Moreno-Manzano, Human-induced neural and mesenchymal stem cell therapy combined with a curcumin nanoconjugate as a spinal cord injury treatment, Int. J. Mol. Sci. 22 (11) (2021) 5966, https://doi.org/10.3390/ijms22115966.

[39] J. Ruzicka, N. Romanyuk, K. Jirakova, A. Hejcl, O. Janouskova, L.U. Machova, M. Bochin, M. Pradny, L. Vargova, P. Jendelova, The effect of iPS-derived neural progenitors seeded on laminin-coated pHEMA-MOETACl hydrogel with dual porosity in a rat model of chronic spinal cord injury, Cell Transplant. 28 (4) (2019) 400–412, https://doi.org/10.1177/0963689718823705.

[40] K.S. Straley, C.W. Foo, S.C. Heilshorn, Biomaterial design strategies for the treatment of spinal cord injuries, J. Neurotrauma 27 (1) (2010) 1–19, https://doi.org/10.1089/neu.2009.0948.

[41] W. Joo, S. Hippenmeyer, L. Luo, Neurodevelopment. Dendrite morphogenesis depends on relative levels of NT-3/TrkC signaling, Science 346 (6209) (2014) 626–629, https://doi.org/10.1126/science.1258996.

[42] G. Li, M.T. Che, X. Zeng, X.C. Qiu, B. Feng, B.Q. Lai, H.Y. Shen, E.A. Ling, Y.S. Zeng, Neurotrophin-3 released from implant of tissue-engineered fibroin scaffolds inhibits inflammation, enhances nerve fiber regeneration, and improves motor function in canine spinal cord injury, J. Biomed. Mater. Res. 106 (8) (2018) 2158–2170, https://doi.org/10.1002/jbm.a.36414.

[43] Z. Wang, H. Duan, F. Hao, P. Hao, W. Zhao, Y. Gao, Y. Gu, J. Song, X. Li, Z. Yang, Circuit reconstruction of newborn neurons after spinal cord injury in adult rats via an NT3-chitosan scaffold, Prog. Neurobiol. 220 (2023) 102375, https://doi.org/10.1016/j.pneurobio.2022.102375.

[44] G. Li, B. Zhang, J.H. Sun, L.Y. Shi, M.Y. Huang, L.J. Huang, Z.J. Lin, Q.Y. Lin, B. Q. Lai, Y.H. Ma, B. Jiang, Y. Ding, H.B. Zhang, M.X. Li, P. Zhu, Y.Q. Wang, X. Zeng, Y.S. Zeng, An NT-3-releasing bioscaffold supports the formation of TrkC-modified neural stem cell-derived neural network tissue with efficacy in repairing spinal cord injury, Bioact. Mater. 6 (11) (2021) 3766–3781, https://doi.org/10.1016/j.bioactmat.2021.03.036.

[45] S. Plantman, M. Patarroyo, K. Fried, A. Domogatskaya, K. Tryggvason, H. Hammarberg, S. Cullheim, Integrin-laminin interactions controlling neurite outgrowth from adult DRG neurons in vitro, Mol. Cell. Neurosci. 39 (1) (2008) 50–62, https://doi.org/10.1016/j.mcn.2008.05.015.

[46] M.A. Anderson, J.E. Burda, Y. Ren, Y. Ao, T.M. O'Shea, R. Kawaguchi, G. Coppola, B.S. Khakh, T.J. Deming, M.V. Sofroniew, Astrocyte scar formation aids central nervous system axon regeneration, Nature 532 (7598) (2016) 195–200, https://doi.org/10.1038/nature17623.

[47] M.V. Sofroniew, Dissecting spinal cord regeneration, Nature 557 (7705) (2018) 343–350, https://doi.org/10.1038/s41586-018-0068-4.

[48] X. Liang, Y. Ding, F. Lin, Y. Zhang, X. Zhou, Q. Meng, X. Lu, G. Jiang, H. Zhu, Y. Chen, Q. Lian, H. Fan, Z. Liu, Overexpression of ERBB4 rejuvenates aged mesenchymal stem cells and enhances angiogenesis via PI3K/AKT and MAPK/ERK pathways, Faseb. J. 33 (3) (2019) 4559–4570, https://doi.org/10.1096/fj.201801690R.

[49] H. Wang, W. Chen, Z. Dong, G. Xing, W. Cui, L. Yao, W.J. Zou, H.L. Robinson, Y. Bian, Z. Liu, K. Zhao, B. Luo, N. Gao, H. Zhang, X. Ren, Z. Yu, J. Meixiong, W. C. Xiong, L. Mei, A novel spinal neuron connection for heat sensation, Neuron 110 (14) (2022) 2315–2333 e6, https://doi.org/10.1016/j.neuron.2022.04.021.

[50] K. Kang, P. Xu, M. Wang, J. Chunyu, X. Sun, G. Ren, W. Xiao, D. Li, FGF21 attenuates neurodegeneration through modulating neuroinflammation and oxidant-stress, Biomed. Pharmacother. 129 (2020) 110439, https://doi.org/10.1016/j.biopha.2020.110439.

[51] W. Liu, B. Xu, S. Zhao, S. Han, R. Quan, W. Liu, C. Ji, B. Chen, Z. Xiao, M. Yin, Y. Yin, J. Dai, Y. Zhao, Spinal cord tissue engineering via covalent interaction between biomaterials and cells, Sci. Adv. 9 (6) (2023) eade8829, https://doi.org/10.1126/sciadv.ade8829.

[52] Z. Chen, Z. Sun, Y. Fan, M. Yin, C. Jin, B. Guo, Y. Yin, R. Quan, S. Zhao, S. Han, X. Cheng, W. Liu, B. Chen, Z. Xiao, J. Dai, Y. Zhao, Mimicked spinal cord fibers trigger axonal regeneration and remyelination after injury, ACS Nano (2023), https://doi.org/10.1021/acsnano.3c09892. Epub ahead of print.